

Emulating optical cycling centers in polyatomic molecules

Ming Li,¹ Jacek Kłos,^{1,2} Alexander Petrov,^{1,3} and Svetlana Kotochigova^{1,*}

¹*Department of Physics, Temple University,*

Philadelphia, Pennsylvania 19122, USA

²*Department of Chemistry and Biochemistry,*

University of Maryland, College Park, Maryland 20742, USA

³*NRC, Kurchatov Institute PNPI, Gatchina,*

188300, and Division of Quantum Mechanics,

St. Petersburg State University, St. Petersburg, 199034, Russia

(Dated: December 4, 2019)

An optical cycling center (OCC) is a recently coined term to indicate two electronic states within a complex quantum object that can repeatedly experience optical laser excitation and spontaneous decay, while being well isolated from its environment. Here we present a quantitative understanding of electronic, vibrational, and rotational excitations of the polyatomic SrOH molecule, which possesses a localized OCC near its Sr atom. In particular, we describe the vibrationally-dependent trends in the Franck-Condon factors of the bending and stretching modes of the molecular electronic states coupled in the optical transition. These simulations required us to perform electronic structure calculations of the multi-dimensional potential energy surfaces of both ground and excited states, the determination of vibrational and bending modes, and corresponding Franck-Condon factors. We also discuss the extent to which the optical cycling center has diagonal Franck-Condon factors.

* skotoch@temple.edu

Laser cooling and trapping of atoms, enabled by the existence of closed optical cycling transitions, have revolutionized atomic physics and led to breakthroughs in several disciplines of science and technology [1]. These advances enabled the simulation of exotic phases in quantum-degenerate atomic gases, the creation of a novel generation of atomic clocks, matter-wave interferometry, and the development of other highly-sensitive sensors. Temperatures below tens of microkelvin have also allowed the confinement of diatomic molecules, built from or associated with laser-cooled atoms, in electric, magnetic, and/or optical traps, where they are isolated from their environment and can be carefully studied.

Achieving similar temperatures for polyatomic molecules, however, remains challenging. Since polyatomic molecules are characterized by multiple degrees of freedom and have correspondingly more complex structures, it is far from obvious whether there exists polyatomic molecules that have the nearly-closed optical cycling transitions required for successful laser cooling. Such transitions could then repeatedly scatter photons.

A diverse list of promising applications for ultracold polyatomic molecules exists. This includes creating novel types of sensors, advancing quantum information science, simulation of complex exotic materials, performing precision spectroscopy to test the Standard Model of particle physics, and, excitingly, the promise of control of quantum chemical reactions when each molecule is prepared in a unique rovibrational quantum state. Moreover, the de Broglie wavelength of colliding ultracold molecules is much larger than the range of intermolecular forces and, thus, the science of the breaking and making of chemical bonds has entered into an unexplored regime.

Over the decades many spectroscopic studies of molecules consisting of an alkaline-earth metal atom (M) and a ligand have been performed [2–10], predominantly to determine their structure. The simplest polyatomic molecules of this type, the triatomic alkaline-earth monohydroxides M-OH, have attracted particular attention after the discovery of their peculiar ionic chemical bond. When a ground-state alkaline-earth atom is bound to OH one of its two outer-most ns^2 electrons is transferred to the ligand, leaving the second electron in an open shell molecular orbital localized around the metal atom. This electron can be optically excited without disturbing the atom-ligand bond leading to so-called highly-diagonal FCFs and efficient optical cycling. High-resolution laser-spectroscopy experiments on CaOH (and CaOD) [5] and SrOH (and SrOD) [11] were first to deduce the strong ionic character of the metal-hydroxide bond. Reference [12] showed that the remaining valence

electron of the metal atom can be easily promoted to any excited orbital.

Recently, Doppler laser cooling [13] of the simpler CaF, SrF, YbF, and YO dimers has been demonstrated [14–18]. Their success is associated with nearly-diagonal Franck-Condon factors (FCFs) on an allowed optical molecular transition. Diagonal FCFs ensure that spontaneous emission from vibrational state v of the excited electronic state populates with near unit probability vibrational state $v' = v$ of the ground electronic state. This closed two-level system can absorb and emit thousands of photons per molecule to achieve cooling.

Following these successful molecular cooling experiments, Isaev and Berger [19] suggested that similar near-diagonality of FCFs exists in other classes of polyatomic molecules. It is now understood that metal-monohydroxides and even larger metal-monoalkoxide molecules with metal atom as Sr, Ca, or Ba are promising candidates for laser cooling. In 2017 the first optical cycling transitions in the polyatomic monohydroxide molecule SrOH was demonstrated by Dr. Doyle’s group [20]. They succeeded in reducing the translational motion of SrOH to the record low temperature of 750 microkelvin starting from 50 milikelvin and using the near unit values of the FCFs. To eliminate rotational branching during the photon cycling process experimentalists use of the rotationally closed $J'' \rightarrow J' - 1$ angular momentum transitions (see for details Refs. [20, 21]).

A significant effort from the scientific community, however, is needed to identify and study the classes of polyatomic molecules with closed optical cycling transitions. Laser cooling of polyatomic molecules is relevant to those molecules that are able to scatter hundreds of photons (stimulated absorption followed by a spontaneous emission) between two vibrational states without loss to other vibrational states, i.e. have a cycling transition where for each cycle the kinetic energy of the molecule is reduced by $\Delta E/k = 1 \mu\text{K}$ and $10 \mu\text{K}$ depending on the cooling process and k is the Boltzmann constant. The requirement of 100 scattering cycles is to a certain degree arbitrary but reasonable and implies that FCF larger than 0.99 are needed. A larger FCF will allow better cooling.

In fact, a comprehensive analysis of level structures that are amenable to laser cooling has to be conducted. Special attention must be given to finding excited-state molecular potentials that have: i) a shape that is similar to that of the ground-state potential; ii) a strong dipole electronic transition with the ground state; and iii) weak transitions to dark states that are not optically coupled to the excited state. It is to be expected that only a small number of polyatomic molecules have these three properties.

An engineering approach, however, can be used to add optical cycling centers (OCCs) to a variety of polyatomic molecules with increasing complexity [22]. For this approach to work we need to ensure that the electrons holding the optically active atom and the molecule together remain sufficiently localized so that the whole molecular system can be translationally cooled. This stringent requirement motivates our intent to conduct an assessment of the role of electron density and localization in the coupling to the ligand molecule. Recent theoretical studies on the cooling properties of alkaline-earth monohydroxides other than SrOH can be found in Refs. [19, 23]. They only determined molecular parameters and Frank-Condon factors for vibronic transitions between ground and excited states near equilibrium geometries.

Our objectives are to better quantify the extent to which polyatomic SrOH is an ideal platform for cooling with laser light as well as to determine the “global” shape of its ground and excited potential energy surfaces (PES) in anticipation of future research on dissociating SrOH into Sr and OH and on ultracold scattering between Sr and OH. In this paper, we describe a complex electronic structure determination of local and some global properties of four multi-dimensional intramolecular PESs of SrOH as well as calculate their corresponding vibrational structures. Our effort involves locating potential minima, potential avoided crossings as well as conical intersections (CIs), where two adiabatic PESs of the same electronic symmetry touch. We represent the PESs and thus the CIs both in terms of adiabatic and diabatic representations. We also determine Frank-Condon factors for not-only the lowest vibrational states but also higher-excited vibrational states of the potentials, where the transitions are no longer diagonal due to non-adiabatic and anharmonic corrections. At near linear geometries, we evaluate the Renner-Teller (RT) parameter [24] for some excited-state potentials.

Results

Electronic potentials of SrOH. The computation of PESs is crucial for defining the landscape in which the nuclei transverse upon interacting with one another. These surfaces can have many features in the context of their topology that are important for the internal transition mechanisms. We begin by describing our calculation of the ground and excited PESs of strontium monohydroxide SrOH. Past theoretical studies on M-OH were devoted to either spectroscopic characteristics near equilibrium geometries [25] or the PESs for the

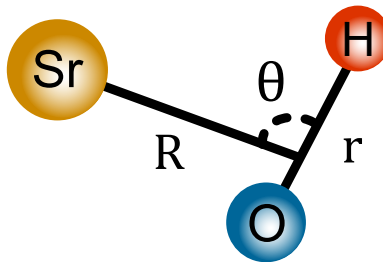


FIG. 1. Illustration of the relevant Jacobi coordinates \mathbf{R} and \mathbf{r} for SrOH. Here, R is the separation between Sr and the center of mass of OH, r is the separation between O and H, and θ is the angle between vectors \mathbf{R} and \mathbf{r} .

lighter BeOH and MgOH with fixed O-H separation [26]. Experimental studies of CaOH [10] and SrOH [2, 7, 8] predominantly focussed on their near-equilibrium ro-vibrational structure.

The relevant multi-dimensional PESs have been determined using a combination of coupled-cluster (CCSD(T)), equation-of-motion coupled-cluster (EOM-CC), and multi-reference configuration interaction (MRCI) methods. This combination allows us to overcome the limitations of the CCSD(T) and EOM-CC methods associated with their single reference nature and the MRCI method with its limits on the size of active space and characterize multiple avoided crossings between relevant PESs. Since the molecule contains one heavy atom, relativistic effects are embedded into the description of the core electrons. Potentials are presented in the Jacobi coordinates \mathbf{R} and \mathbf{r} defined in Fig. 1. For our purposes it is sufficient to determine the PESs, which are only functions of (R, θ, r) in the two-dimensional plane with the OH separation fixed to its diatomic equilibrium separation as the energy required to vibrationally excite OH is nearly seven times larger than those of the Sr-OH stretch and bend. Coupling to the OH stretch can then be ignored for our objectives. (We always use $r = 1.832a_0$ and also suppress the r dependence in our notation.)

The PESs and corresponding electronic wavefunctions are labeled by their total electronic spin angular momentum, here always a doublet or spin 1/2, as well as the irreducible representations of point groups $C_{\infty v}$ for linear geometries and C_s otherwise. In particular, we obtain four ${}^2A'$ and two ${}^2A''$ potentials using standard notation for the irreducible representations of C_s , respectively. For linear geometries ${}^2A'$ states connect to either ${}^2\Sigma^+$ or ${}^2\Pi$ states of the $C_{\infty v}$ symmetry group, while ${}^2A''$ states always become ${}^2\Pi$ states. Hence, we label

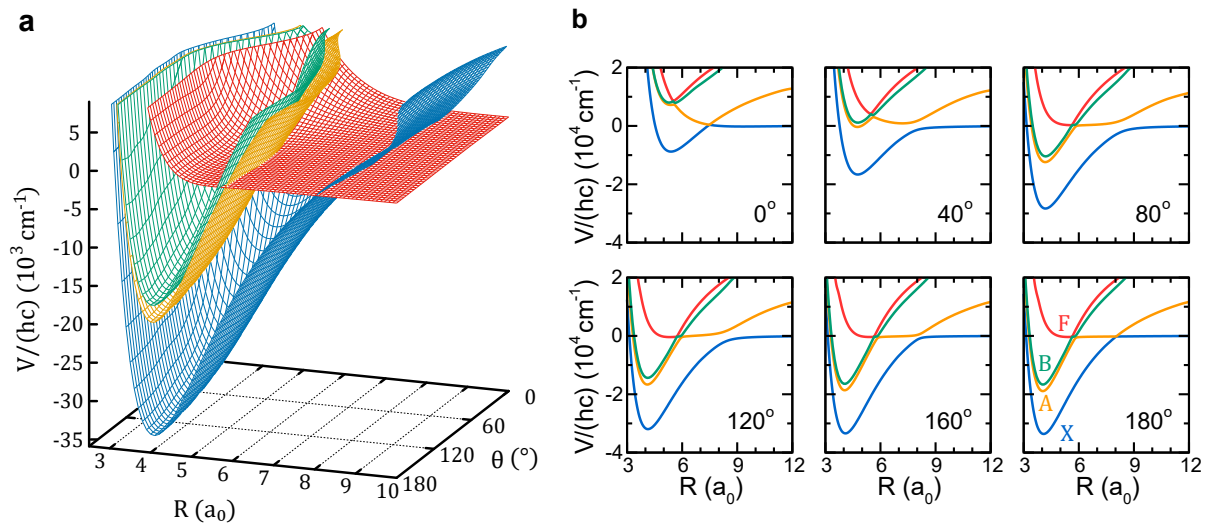


FIG. 2. The ground and excited potential energy surfaces $V(R, \theta)$ of SrOH at separation $r = 1.832a_0$. a) A two-dimensional cut through the four relevant ${}^2A'$ diabatic potential surfaces as functions of separation R and angle θ . The blue, orange, green, and red curves correspond to states $1\,{}^2A'(X^2\Sigma^+)$, $2\,{}^2A'(A^2\Pi)$, $3\,{}^2A'(B^2\Sigma^+)$, and $4\,{}^2A'(F^2\Pi)$, respectively. Seams, containing conical intersections at the two linear geometries, are lines along which two diabatic potentials are degenerate. b) Adiabatic ${}^2A'$ potentials as functions of separation R for six values of angle θ . The absolute ground state minimum occurs at angle $\theta = 180^\circ$ at separation $R \approx 4a_0$. The zero of energy is set at the energy of a ground-state Sr atom infinitely far away from the ground-state OH($X^2\Pi$) molecule at its equilibrium bond length. Potential energies are expressed in units of cm^{-1} , using Planck's constant h and speed of light in vacuum c .

potential surfaces by $n\,{}^2A''(m\,{}^2\Lambda^\pm)$, where $n = 1, 2, 3, \dots$ and $m = X, A, B, \dots$ indicate the energy ordering of states for R and r close to their equilibrium separations and $\theta = 180^\circ$.

CCSD(T) and EOM-CC calculations lead to the most-accurate PESs for each irreducible representation and, in principle, should return the corresponding adiabatic PES with avoided crossings from excited potentials in the same irreducible representations. Numerically, however, we find this not to be true due to the fact that the method use only excitations from a single reference configuration and that the electronic wavefunctions rapidly change from ionic to covalently bonded with small changes in the Jacobi coordinates, in particular regions of R . In essence, for a given reference configuration the CCSD(T) or EOM-CC simulations

return diabatic potentials with electronic wavefunctions that have either an ionic bond, where one of the outer valence electrons of Sr is now tightly bound to oxygen, or a covalent bond, where both valence electrons mostly remain in orbit around the Sr nucleus and barely couple with the OH electron cloud. The diabatic PESs have lines in the plane (R, θ) along which two potentials have the same energy.

Figure 2a shows four diabatic PESs of SrOH as functions of R and θ obtained by CCSD(T) and EOM-CC methods. Details regarding electronic basis sets, coupled-cluster method for the individual ${}^2A'$ and ${}^2A''$ PESs, and interpolation can be found in Methods. The calculations are performed at ten angular and about 45 radial geometries. This data is then interpolated using an analytical functional form. The interpolated PESs are essential in recognizing system characteristics, such as minima and transition states, i. e. saddle points, as well as crossings. Near extrema the curvature or Hessian matrix is evaluated.

The optimized geometry for the ground-state SrOH molecule occurs at $\theta = 180^\circ$. Its electronic wavefunction has $X^2\Sigma^+$ symmetry and is ionically bonded. These observations are consistent with spectroscopic data [27] and the semi-empirical analyses of Ref. [28]. The $2^2A'$ and $3^2A'$ states also have ionic character and minima at $\theta = 180^\circ$. In fact, the minima of these three potentials have nearly the same equilibrium coordinates and curvatures providing excellent conditions for optical cycling. These conditions are further described in subsection “Wavefunction overlaps”.

The fourth diabatic PES is the shallow excited $4^2A'(F^2\Pi)$ potential with a covalently bonded electronic state that dissociates to Sr(1S) and OH($X^2\Pi$). For large R the ionic PESs correlate to electronically-excited states of the Sr atom. Crucially, we observe that the three ionic diabatic PESs each have a curved line in the (R, θ) plane along which the $4^2A'(F^2\Pi)$ potential equals the energy of the ionic potential. It is worth noting that to good approximation this curve is independent of θ . The $4^2A'(F^2\Pi)$ potential is expected to play a crucial role in the zero-energy dissociation of SrOH to create ultracold OH fragments, an important radical for various scientific applications.

Figure 2b shows the interpolated adiabatic ${}^2A'$ PESs of the SrOH molecule as functions of R for six values of θ and $r = 1.832a_0$ obtained by diagonalizing the 4×4 Hamiltonian with the diabatic PESs as diagonal matrix elements and coupling matrix elements described in subsection “Non-adiabatic couplings and conical intersections” at each (R, θ) . These cuts through the PESs exhibit several intriguing features. First, for $\theta = 0^\circ$ and 180° CIs, where

two potentials still touch, are apparent. For other values of θ the crossings are avoided. The location of the CIs at linear geometries is specific to SrOH, other molecules will have CIs at other geometries. CIs lead to geometric or Berry phases [29], i. e. sign changes associated with an electronic wavefunction when transported along a closed path encircling a CI. These phases lead to interference that allows efficient non-adiabatic transitions between surfaces [30], modify product rotational state distributions in chemical reactions, and influence ro-vibrationally averaged transition matrix elements.

We have similarly obtained two diabatic ${}^2A''$ PESs. Both are ${}^2\Pi$ states at linear $C_{\infty v}$ geometries. On the energy scale of Fig. 2a their shapes are nearly indistinguishable from those of the $2\,{}^2A'(A^2\Pi)$ and $4\,{}^2A'(F^2\Pi)$ potentials. In fact, $1\,{}^2A''(A^2\Pi)$ and $2\,{}^2A'(A^2\Pi)$ as well as $2\,{}^2A''(F^2\Pi)$ and $4\,{}^2A'(F^2\Pi)$ are degenerate for linear geometries. Unlike the corresponding ${}^2A'$ potentials, however, the two ${}^2A''$ potentials do not possess CIs.

Non-adiabatic couplings and conical intersections. The adiabatic ${}^2A'$ PESs in Fig. 2b are Born-Oppenheimer (BO) potentials [31] that are typically used as a starting point in describing scattering and chemical processes. The BO approximation is based on the realization that the motion of nuclei and electrons occur on different time or energy scales and usually only a single PES is required. This leads to a significant simplification of the description of scattering and chemical processes.

For SrOH the BO approximation breaks down when potentials of ${}^2A'$ symmetry come close and even become degenerate for one or more geometries. Couplings between these potentials can not then be neglected. The corresponding non-adiabatic transition probability for “hopping” between potentials increases dramatically especially for conical intersections and can greatly affect chemical properties [32].

Our CCSD(T) and EOM-CC calculations only resulted in diabatic PESs $V_m(R, \theta)$ and electronic wavefunctions $|\phi_m\rangle$, due to their reliance on a single reference configuration. Here, index m labels states and corresponding PESs. As the diabatic electronic wavefunctions are predominantly described by this single reference configuration, their dependence on R and θ is weak and negligible, and suppressed in our notation.

Coupling matrix elements between the diabatic potentials are constructed by performing less-accurate MRCI calculations at the SD level with a basis set similar to that used for our CCSD(T) calculations (details are given in Methods.) Our MRCI calculations rely on

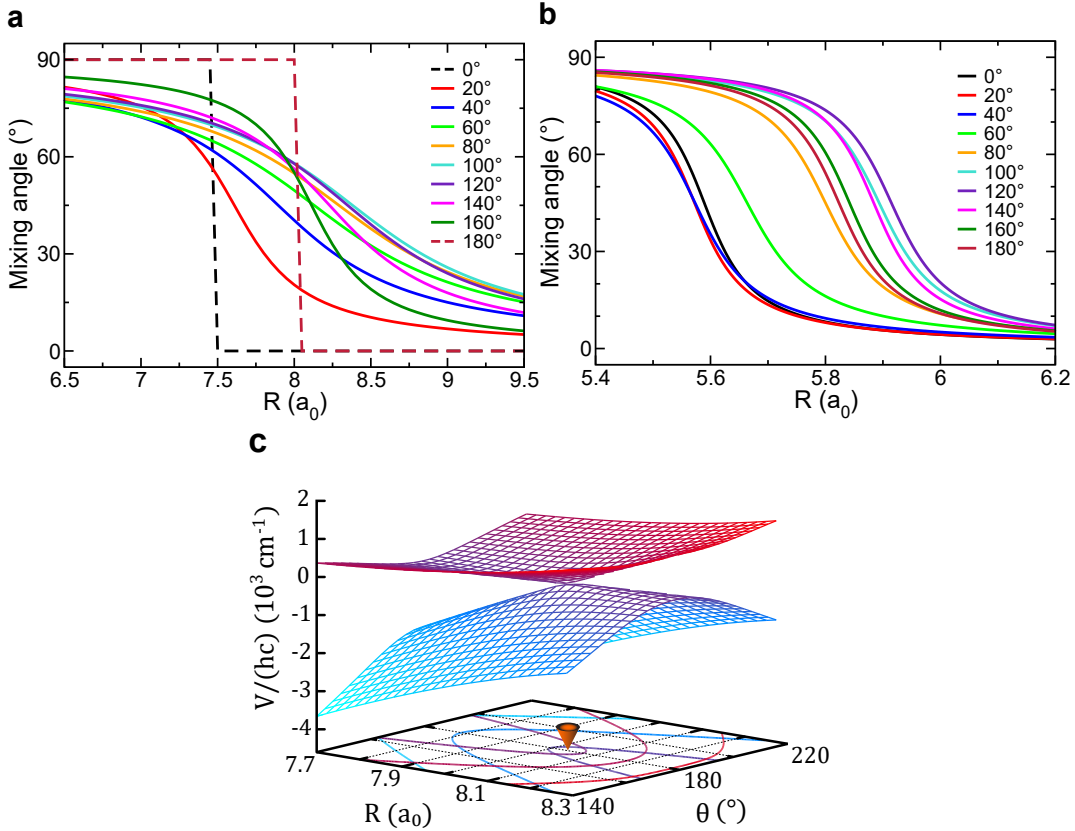


FIG. 3. Characterization of mixing angles and conical intersections between the $1^2A'$ and $4^2A'$ states. a) Mixing angles $\vartheta(R, \theta)$ for the diabatic $1^2A'$ and $4^2A'$ states as functions of separation R for ten different values of angle θ determined from our quantum-mechanical calculations. Conical intersections are apparent as the -90° jump in mixing angle for curves with $\theta = 0^\circ$ and 180° . b) Mixing angles similarly determined from our calculations for the $1^2A''$ and $2^2A''$ diabatic states. No conical intersection is present. c) Adiabatic $1^2A'$ (blue surface) and $4^2A'$ (red surface) potential energy surfaces V as functions of separation R and angle θ near the conical intersection at $R \approx 8a_0$ and $\theta = 180^\circ$.

two or more reference configurations and thus do lead to adiabatic BO potentials $U_n(R, \theta)$ and adiabatic electronic wavefunctions $|\psi_n(R, \theta)\rangle$, where index n labels states. Adiabatic wavefunctions strongly depend on R and θ near crossings or avoid crossings between potentials. We also compute diagonal overlap matrix elements $\langle \psi_n(R', \theta') | \psi_n(R, \theta) \rangle$ at different geometries within the MRCI method.

Numerically, we find that the general shapes of the CCSD(T) and MRCI potentials are the

same. Specifically, the geometries where diabatic potentials in Fig. 2a cross and adiabatic MRCI potentials avoid are in good agreement. We can then assume that away from the crossings $|\psi_n(R, \theta)\rangle \approx |\phi_m\rangle$ for some diabatic index m . Near avoided crossings the adiabatic wavefunction is a superposition of diabatic wavefunctions.

We focus on the coupling matrix element between the diabatic $1^2A'$ and $4^2A'$ states near $R = 8a_0$ as well as those between $1^2A''$ and $2^2A''$ near $R = 6a_0$. We assume the coupling between the diabatic $2^2A'$ and $4^2A'$ states near $R = 6a_0$ is the same as between the A'' ones. For each pair of states the adiabatic wavefunctions can then be approximated as the superposition [33]

$$\begin{pmatrix} |\psi_n(R, \theta)\rangle \\ |\psi_{n'}(R, \theta)\rangle \end{pmatrix} = \begin{pmatrix} \cos \vartheta(R, \theta) & \sin \vartheta(R, \theta) \\ -\sin \vartheta(R, \theta) & \cos \vartheta(R, \theta) \end{pmatrix} \begin{pmatrix} |\phi_m\rangle \\ |\phi_{m'}\rangle \end{pmatrix} \quad (1)$$

with indices n, n' and m, m' , respectively, where mixing angle $\vartheta(R, \theta)$ is to be determined.

To determine the mixing angle we, first, identify a reference geometry R_{ref} for each θ away from the crossings, where $|\psi_n(R_{\text{ref}}, \theta)\rangle \approx |\phi_m\rangle$, $|\psi_{n'}(R_{\text{ref}}, \theta)\rangle \approx |\phi_{m'}\rangle$, and we can assume $\vartheta(R_{\text{ref}}, \theta) = 0$. The mixing angle at other radial geometries is then given by

$$\vartheta(R, \theta) = \arccos [\langle \psi_n(R_{\text{ref}}, \theta) | \psi_n(R, \theta) \rangle] \quad (2)$$

and the coupling matrix element between the two diabatic states m and m' is

$$W_{mm'}(R, \theta) = \frac{1}{2} [V_m(R, \theta) - V_{m'}(R, \theta)] \tan[2\vartheta(R, \theta)]. \quad (3)$$

In the limit $V_m(R, \theta) \rightarrow V_{m'}(R, \theta)$ this expression needs to be treated carefully. The mixing angle will approach $\pi/4$ and only at CIs $W_{mm'}(R, \theta) = 0$.

In practice, we parametrize $\vartheta(R, \theta)$ as we perform MRCI calculations only on a restricted set of geometries (R_i, θ_j) . We ensure a smooth functional dependence on R at fixed θ by using

$$\vartheta(R, \theta) = -\frac{1}{2} \arctan \left[\frac{R - R_c(\theta)}{R_0(\theta)} \right] + \frac{\pi}{4}, \quad (4)$$

where $R_c(\theta)$ is the curve where $V_m(R, \theta) = V_{m'}(R, \theta)$ and $R_0(\theta) \geq 0$ is a coupling width that is fitted to reproduce the MRCI overlap matrix at θ_j (at other θ it is found with the Akima interpolation method [34].) By construction $R_0(\theta)$ is much smaller than $|R_{\text{ref}} - R_c(\theta)|$. We use $R_{\text{ref}} = 11a_0$ and $7a_0$ for the pair of $2A'$ and $2A''$ states, respectively. Values for θ_j , R_c , and R_0 are available upon request.

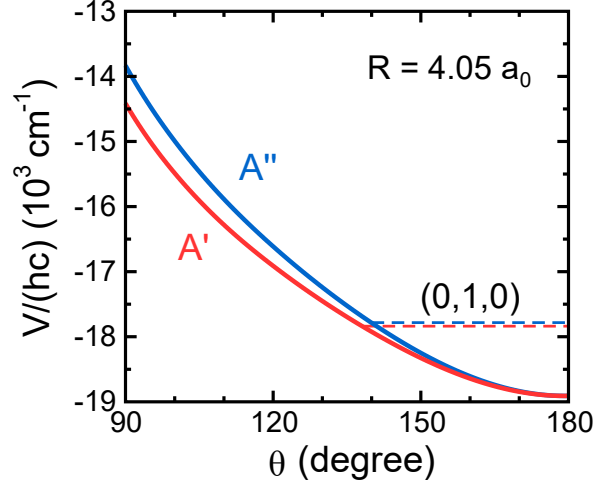


FIG. 4. The splitting of $2^2A'$ and $1^2A''$ potential energy surfaces V as functions of angle θ at the separations $R = 4.05a_0$ and $r = 1.832a_0$. The potentials are degenerate at $\theta = 180^\circ$. Dashed lines indicate the calculated energies of the first excited bending modes $(0, 1, 0)$ for the two potentials, respectively.

Figures 3a and b show mixing angles $\vartheta(R, \theta)$ for the two diabatic $2^2A'$ and the two $2^2A''$ states, respectively. In both panels the mixing angle is seen to change relatively rapidly over a small range of R , i. e. determined by $R_0(\theta)$, from nearly 90° to 0° . When $\vartheta(R, \theta) = 45^\circ$ we have $R = R_c(\theta)$. For the $2^2A'$ states in panel a, $R_0(\theta)$ is largest for $\theta \approx 90^\circ$ and is zero for $\theta \rightarrow 0^\circ$ and 180° , indicative of CIs where $\vartheta(R, \theta)$ has an infinitely sharp jump from 90° to 0° . For the $2^2A''$ states in panel b the width $R_0(\theta)$ is nearly independent of θ and there is no CI. Finally, Fig. 3c shows the adiabatic $2^2A'$ potentials near the CI at $R \approx 8a_0$ and $\theta = 180^\circ$ as determined by diagonalizing the 2×2 matrix containing the relevant diabatic PESs coupled by the coupling matrix element at each (R, θ) . The figure corresponds to a surface plot of the data shown in Fig. 2b.

The Renner-Teller effect [35, 36] occurs in linear or quasi-linear, open-shell triatomic molecules and relies on non-adiabatic coupling between rovibrational and electronic motion in polyatomic molecules. It is associated with an energy degeneracy of electronic states for high-symmetry geometries that is lifted by vibrational bending motion. The motion causes degenerate potential energy surfaces to split and breaks the Born-Oppenheimer (BO) approximation. Stretching modes, which do not break linear symmetry, are not affected.

We calculate the RT parameter by estimating the non-adiabatic coupling between $2^2A'$

and $1^2A''$ PESs. These PESs are degenerate at co-linear geometries but split otherwise.

Figure 4 shows the potentials near the co-linear equilibrium separation R as functions of the bending angle θ . The potentials are degenerate at $\theta = 180^\circ$. The slight anisotropy away from linear geometry causes the bending vibrational motion in the two PESs to differ. Our calculated $(0, 1, 0)$ bending energy relative to $(0, 0, 0)$ for the $2^2A'$ and $1^2A''$ states are $\omega(A') = 384 \text{ cm}^{-1}$ and $\omega(A'') = 412 \text{ cm}^{-1}$, respectively, corresponding to a 28 cm^{-1} difference. In the harmonic approximation this differential splitting is characterized by the Renner-Teller parameter [27]

$$\epsilon = \frac{\omega(A')^2 - \omega(A'')^2}{\omega(A')^2 + \omega(A'')^2} = -0.0693. \quad (5)$$

Presunka & Coxon [27] estimated a Renner-Teller parameter of -0.0791 for these states from fitting this and other non-adiabatic parameters to spectroscopic data. Here, we calculate ϵ for the first time from *ab-initio* calculations and find agreement with spectroscopic estimate to within 15%.

Wavefunction overlaps. Laser cooling of SrOH [20] relied on optical cycling transitions between either $X^2\Sigma^+ \leftrightarrow A^2\Pi$ or $X^2\Sigma^+ \leftrightarrow B^2\Sigma^+$ vibronic states. The success of the experiment is associated with near-diagonal FCFs between the sets of levels supported by these electronic potentials, which ensures that spontaneous emission from a rovibrational state of the excited electronic state populates with near unit probability the corresponding rovibrational state of the ground electronic state. This two-level system absorbs and emits many photons to achieve cooling [13].

Table I shows atomic orbital composition for the ground and A and B electronically excited states of SrOH. The X electronic ground state is mostly described by Sr- s orbital as expected. One can notice that in the case of the A and B states there is some participation of d -orbitals of Sr atom. For the A state that participation is quite small and the excited state is mainly formed by Sr- p orbital participating in $s - p$ transition. The B state has quite a substantial component originating from Sr- d -orbitals indicating increased $s - d$ type hybridization with some participation of O- s and H- s atomic orbitals.

Our computation of vibrational wavefunctions and their overlap for electronic transitions is described in Methods. We focus on vibrational levels near the global minima of the diabatic PESs at $\theta = 180^\circ$ as shown in Fig. 5. Effects from diabatic couplings, CIs, fine-

TABLE I. Orbital composition analysis for the ground $X^2\Sigma^+$ and lowest lying electronic $A^2\Pi$ and $B^2\Sigma^+$ states of the SrOH molecule. For each of the three molecular states columns correspond to amplitudes of the s , p , and d valence orbitals of the strontium cation (Sr- s , Sr- p , Sr- d), the s valence orbital of oxygen (O- s), and the s orbital of hydrogen (H- s).

State	Sr- s	Sr- p	Sr- d	O- s	H- s
$X^2\Sigma^+$	0.9	0.1	-	-	-
$A^2\Pi$	-	0.9	0.1	-	-
$B^2\Sigma^+$	-0.2	0.2	0.4	0.3	0.3

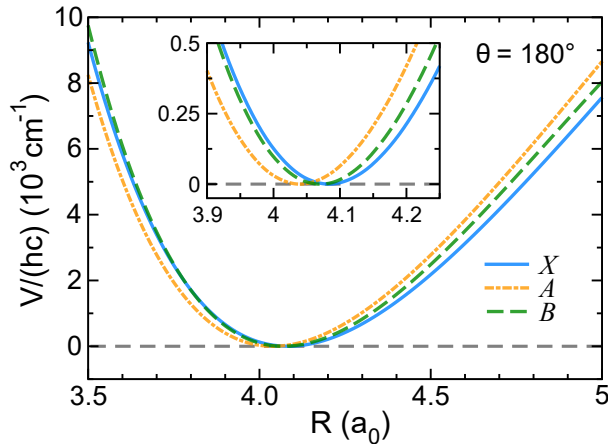


FIG. 5. Overlay of the ground and excited electronic potential energies V as functions of separation R at angle $\theta = 180^\circ$, linear geometry. The inset shows a blowup of the potential minima.

structure interactions, and coriolis forces among the A' and A'' surfaces can then be omitted. The lowest vibrational and rotational states are uniquely labeled by the three vibrational quantum numbers v_s , v_b , and v_{OH} , total trimer orbital angular momentum J , and parity p . Here, the vibrational quantum numbers correspond to the Sr-O stretch, the Sr-O-H bend, and the O-H stretch, respectively. We use the abbreviated notation $(v_s, v_b, v_{\text{OH}})$ and always have $v_{\text{OH}} = 0$ for frozen separation r . Our vibrational energies are discussed and compared to results from existing literature in Methods.

Evaluation of Frank-Condon factors. Figure 6a examines our diagonal FCFs of stretching modes $(v'_s, v'_b, v'_{\text{OH}}) = (v_s, 0, 0) \rightarrow (v_s, 0, 0)$ among the $J = 1$ $1^2A'(X^2\Sigma^+)$, $J = 0$

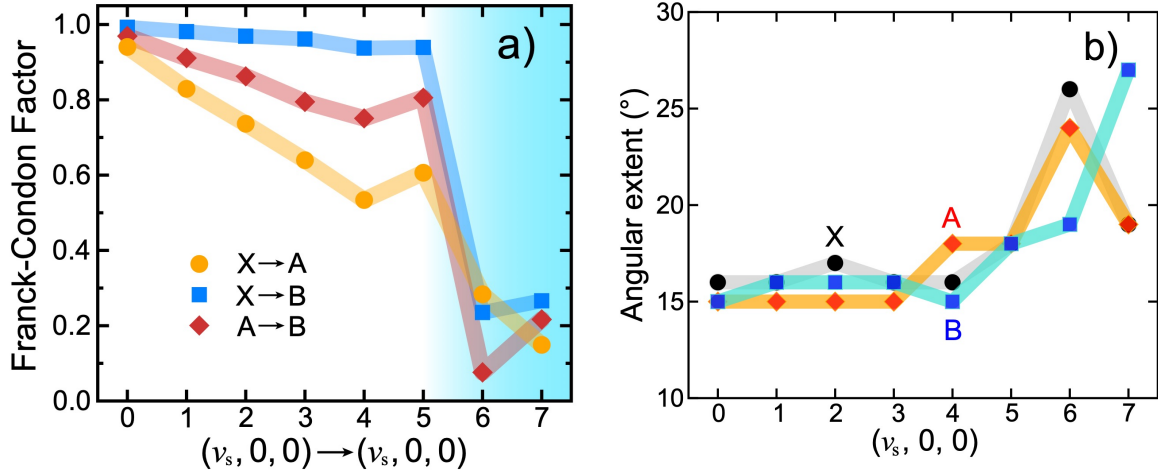


FIG. 6. Characterization of optical cycling transitions as functions of vibrational stretching mode quantum number v_s . a) Diagonal Frank-Condon factors of vibrational transitions among electronic states $1^2A'(X^2\Sigma^+)$, $2^2A'(A^2\Pi)$, and $3^2A'(B^2\Sigma^+)$ as functions of vibrational states $(v'_s, v'_b, v'_{OH}) = (v_s, 0, 0) \rightarrow (v_s, 0, 0)$. Transitions are color coded by the linear $C_{\infty v}$ symmetry, i. e. blue, red, and orange curves and markers correspond to the X \rightarrow B, A \rightarrow B, and X \rightarrow A transitions, respectively. The blue shaded area indicates a sudden decrease of Frank-Condon factors for all three vibronic manifolds at $v_s = 6$ and 7 . b) The expected angular extent of the vibrational wave function relative to the angle $\theta = 180^\circ$ equilibrium geometry as a function of the stretching mode quantum number. The larger extent for $v_s > 5$ corresponds to a significant wave function probability away from linearity.

$2^2A'(A^2\Pi)$, and the $J = 0$ $3^2A'(B^2\Sigma^+)$ states. For $v_s \leq 4$ the FCFs decrease linearly with increasing v_s . In this regime, stretching modes with different bending quantum numbers are well separated in energy and FCFs based on the harmonic approximation of the potentials are in reasonable agreement with our more precise evaluation. The FCFs are largest for the $1^2A'(X^2\Sigma^+)$ to $3^2A'(B^2\Sigma^+)$ transition.

We observe a dramatic decrease of the FCFs for $v_s = 6$ and 7 , emphasized by a blue shaded area in Fig. 6a. We explain this behavior in terms of the complex overlap of vibrational wavefunctions in R and θ . Figure 6b shows the expected angular extents of vibrational wavefunctions relative to the $\theta = 180^\circ$ equilibrium linear geometry as functions of v_s . For $v_b = 0$ states the vibrational wavefunctions along θ are nodeless. We observe that the

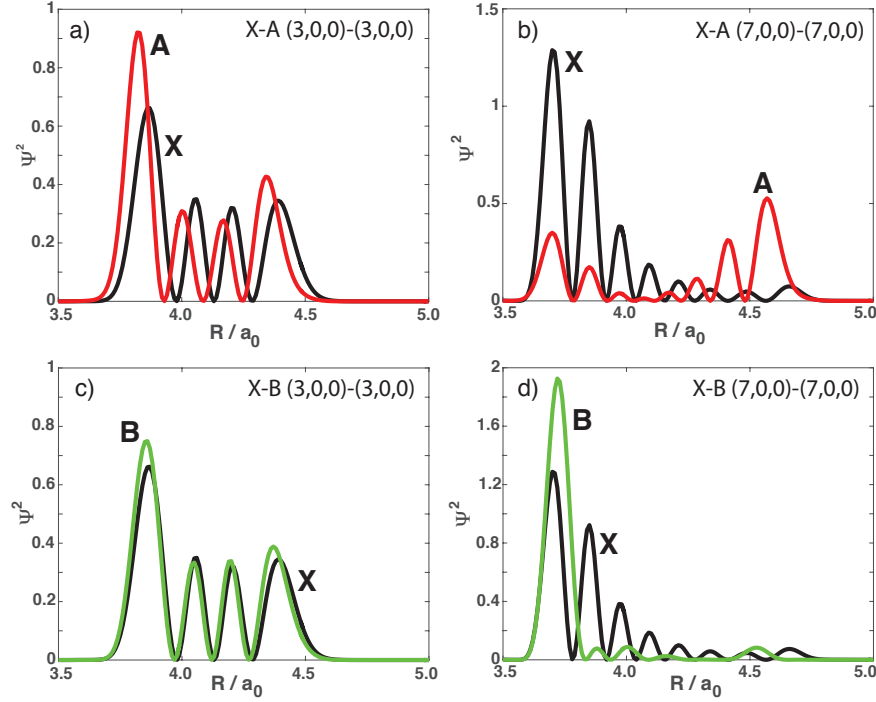


FIG. 7. Square of the vibrational wave function for the stretching modes $(v_s, 0, 0) = (3, 0, 0)$ and $(7, 0, 0)$ as functions of separation R at angle $\theta = 180^\circ$ for the ground $1^2A'(X^2\Sigma^+)$ (black curves) and excited $2^2A'(A^2\Pi)$, and $3^2A'(B^2\Sigma^+)$ (red and green curves) electronic states, respectively. a) Sr-O stretch with $(v_s, 0, 0) = (3, 0, 0)$ in the $X^2\Sigma^+$ and $A^2\Pi$ potentials; b) Sr-O stretch with $(v_s, 0, 0) = (7, 0, 0)$ in the $X^2\Sigma^+$ and $A^2\Pi$ potentials; c) Sr-O stretch with $(v_s, 0, 0) = (3, 0, 0)$ in the $X^2\Sigma^+$ and $B^2\Sigma^+$ potentials; d) Sr-O stretch with $(v_s, 0, 0) = (7, 0, 0)$ in the $X^2\Sigma^+$ and $B^2\Sigma^+$ potentials.

bending range for $v_s < 4$ vibrational levels in all three electronic states is $\approx 15^\circ$ and that for $v_s > 5$ the wavefunction is more extended. In fact, for $v_s > 5$ the angular extent for the $1^2A'(X^2\Sigma^+)$ and $2^2A'(A^2\Pi)$ states remains close but differ significantly from those of the $3^2A'(B^2\Sigma^+)$ state. This irregularity in the $v_b = 0$ series coincides with the corresponding irregularity in FCFs, but clearly is not the whole story as we could conclude that the $1^2A'(X^2\Sigma^+)$ to $2^2A'(A^2\Pi)$ transitions remain diagonal.

Figure 7 compares vibrational wavefunctions as functions of stretching-direction R for linear geometry $\theta = 180^\circ$ for the $1^2A'(X^2\Sigma^+)$ to $2^2A'(A^2\Pi)$ and $1^2A'(X^2\Sigma^+)$ to $3^2A'(B^2\Sigma^+)$ transitions. We observe that for the $(3, 0, 0)$ vibrational level the wavefunction of the three electronic potentials have similar shape, although the overlap for the $1^2A'(X^2\Sigma^+)$ and

$3^2A'(B^2\Sigma^+)$ states is significantly better. For the (7,0,0) level neither overlap is good. Combining our observations on the angular extend in Fig. 6b with those on the stretching direction then explains the dramatic decrease of the FCFs for $v_s = 6$ and 7.

Table II presents our diagonal and off-diagonal FCF matrix elements. For simplicity FCFs smaller than 10^{-3} have been omitted. Overall the $1^2A'(X^2\Sigma^+)$ to $3^2A'(B^2\Sigma^+)$ vibronic transitions have higher diagonal FCFs and smaller off-diagonal FCFs than those for the $1^2A'(X^2\Sigma^+)$ to $2^2A'(A^2\Pi)$ transition. The (0,0,0) to (0,0,0) FCFs for these electronic states was measured in Ref. [28]. They found 0.957(3) and 0.977(2) for the $1^2A'(X^2\Sigma^+)$ to $2^2A'(A^2\Pi)$ and $1^2A'(X^2\Sigma^+)$ to $3^2A'(B^2\Sigma^+)$ transition, respectively. These value are smaller than those found in our calculations. Better agreement might be found by allowing the OH bond to change. Extended tables of the FCF matrices are presented in Supplementary Note 1.

Discussion

We have quantitatively analyzed the unique localized chemical bond between valence electrons of Sr and OH radical. We have shown that one of the two Sr valence electrons remains localized on the Sr^+ cation and can be optically excited without disturbing the atom-ligand bond leading to highly-diagonal FCFs and efficient optical-cycling conditions. The goal of our theoretical work has been to analyze the cooling process based on a rigorous calculation of the electronic structure of this important molecule previously totally unknown, as a means to look into the nature of optical cycling centers in polyatomic molecules and help extend its generality. Furthermore, our work indicates that there are several electronic and vibrational states that can be used for the laser cooling with FCFs close to unity. We also explain why the X-B transitions have more diagonal FCFs than X-A transitions.

Our analysis of the electronic and vibrational energy landscape of SrOH also points to intriguing molecular features that require further explorations. For instance, we located conical intersections in SrOH that can have important implications for non-adiabatic transitions between PESs, collisional dynamics within this molecule, as well as its fragmentation. Our characterization of the geometric Renner-Teller effects provides better understanding of the coupling between electronic and vibrational motion and accounts for the possible nominally-forbidden loss channels.

Finally, Ref. [21] proposed that replacing the hydrogen atom in the monohydroxide with

larger ligand should not significantly disturb the valence electron of metal-cation so that optical cycling and cooling even larger polyatomic molecule might remain possible. Detailed confirmation of this idea also awaits future research.

Methods

Ab initio methods for the SrOH potential energy surfaces. We have used the coupled-cluster CCSD(T) method from CFOUR [37] to calculate the ground and first excited diabatic PESs with total electron spin 1/2 of A' symmetry (ground state), A'' symmetry (first excited state), and the highly excited diabatic PES with spin 1/2 of A'' symmetry but with completely different reference configuration. They are labeled $1^2A'$, $1^2A''$ and $2^2A''$, respectively. The CCSD(T) calculations are based on the atomic bases sets def2-QZVPP (8s8p5d3f)/[7s5p4d3f] [38] paired with the Stuttgart ECP28MDF effective core potential [39] for Sr, the all electron aug-cc-pVQZ (13s7p4d3f2g)/[6s5p4d3f2g] for O, and aug-cc-pVQZ (7s4p3d2f)/[5s4p3d2f] for H [40].

For all excited diabatic potentials, $1^2A''$, $2^2A'$, $3^2A'$, $2^2A''$, and $4^2A'$, we employed the equation-of-motion coupled-cluster (EOM-CCSD(dT)) approach, implemented in Q-CHEM, version 5.0 [41]. The excitation-energy root space for the EOM-CCSD(dT) method spans four roots of A' symmetry and two roots of the A'' symmetry. We use the Stuttgart ECP28MDF relativistic effective core potential [39] along with Peterson’s pseudopotential based, polarized valence, correlation consistent triple-zeta (aug-cc-pVTZ-PP) basis for the Sr atom [42] and corresponding Dunning’s aug-cc-pVTZ basis for the O and H atoms [40]. These calculations allowed us to obtain the relative splittings between A' and A'' PESs and between the $2^2A'$ and $3^2A'$ PESs.

The CC based methods used in construction of the $^2A'$ and $^2A''$ potentials are capable of providing highly accurate quantitative data about PESs. Unfortunately, these methods are unsuitable for the calculation of PESs near their crossing or avoided crossing. The way out is a MRCI calculation, which realistically, can only be done with an active space of limited size.

We characterize non-adiabatic couplings between states by using the MRCI calculations with single and double excitations, implemented in MOLPRO [43]. The ECP28MDF Köln pseudo-potential [39] with the augmented correlation-consistent triple-zeta basis aug-cc-pVTZ-PP [42] for Sr and the all-electron aug-cc-pVQZ basis for O and H [40] are applied.

The calculations are performed with reference orbitals constructed from state-averaged multi-reference self-consistent-field calculations. Finally, all electronic structure calculations were performed with assumption that the OH separation is fixed at $r = 1.832a_0$.

Interpolation of potential energy surfaces. The four ${}^2A'$ and two ${}^2A''$ two-dimensional *diabatic* SrOH potentials have been computed on a grid in Jacobi coordinates R and θ . In order to find the potential energies at other coordinates we expand the angular dependence of each *diabatic* PESs in terms of Legendre polynomials $P_l(\cos \theta)$ via

$$V_{\text{mr}}(R, \theta) = \sum_{l=0}^L U_l(R) P_l(\cos \theta) \quad (6)$$

for $R < 16.5a_0$ with $L = 9$ and radial expansion coefficients $U_l(R)$. For separations $R > 16.5a_0$ the PESs are fit to

$$V_{\text{r}}(R, \theta) = \sum_{n=6}^9 \sum_{l=0}^{n-4} \frac{C_{nl}}{R^n} P_l(\cos \theta) \quad (7)$$

with dispersion coefficients C_{nl} . The radial coefficients $U_l(R)$ and C_{nl} are determined by the Reproducing Kernel Hilbert Space (RKHS) interpolation method [44]. The two expansions are smoothly joined using

$$V(R, \theta) = [1 - f(R)] V_{\text{mr}}(R, \theta) + f(R) V_{\text{r}}(R, \theta) \quad (8)$$

and $f(R) = (1 + \tanh[\alpha(R - R_{\text{sw}})])/2$. The parameter values for describing $U_l(R)$, C_{nl} , α , and R_{sw} are available upon request.

Bound state energies. For each diabatic PESs the corresponding vibrational Hamiltonian includes the kinetic-energy operators for Jacobi coordinates \mathbf{R} and \mathbf{r} with masses $\mu = m_{\text{Sr}}m_{\text{OH}}/(m_{\text{Sr}} + m_{\text{OH}})$ and m_{OH} , respectively. Here, m_{Sr} is the mass of the Sr atom and m_{OH} that of the OH molecule. The vibrational Hamiltonian commutes with the trimer orbital-angular-momentum operator $\mathbf{J} = \mathbf{j} + \mathbf{l}$ as well as the parity operator p , the symmetry under spatial inversion of all electrons and nuclei around the center-of-mass position of the trimer. Here, \mathbf{j} and \mathbf{l} are the orbital-angular-momentum operators of ground-state OH and of Sr relative to the center of mass of OH, respectively.

We diagonalize the vibrational Hamiltonian by first creating a one-dimensional basis of bound states of the radial Hamiltonian $-\hbar^2/(2\mu)d^2/dR^2 + V(R)$ using the distributed Gaussian basis approach and where $V(R)$ is the interpolated PES computed at $\theta = 180^\circ$

and $r = 1.832a_0$ (\hbar is the reduced Planck constant.) Then the vibrational Hamiltonian is diagonalized in the product basis of radial bound states and superpositions of products of spherical harmonic functions for the orientation of \mathbf{R} and \mathbf{r} , such that the basis states are eigenstates of \mathbf{J}^2 , J_z , and parity p .

Within these approximations we have computed several of the energetically-lowest vibrational levels with total angular momentum $J^p = 0^+$ and 1^\pm of the diabatic $1^2A'(X^2\Sigma^+)$, $2^2A'(A^2\Pi)$, $1^2A''(A^2\Pi)$, and $3^2A'(B^2\Sigma^+)$. We focus on these rotational states as $J = 1 \rightarrow J' = 0$ transitions from the $1^2A'(X^2\Sigma^+)$ ground state are used in laser cooling of SrOH [20].

In Table III we compare some of our calculated energies with total angular momentum $J = 0$ to other semi-empirical results as well as experimental data. Our results for the Sr-O stretch and Sr-O-H bend energies agree well with experimental data, even though the OH bond is not allowed to stretch and diabatic couplings are omitted. The energy difference between the $(v_s, v_b, 0) = (1, 0, 0)$ and $(0, 0, 0)$ states, the Sr-O stretching mode, are reproduced to better than 1% for the $1^2A'(X^2\Sigma^+)$ and $1^2A''(A^2\Pi)$ states. The discrepancy increases to 2.5% for the $3^2A'(B^2\Sigma^+)$ state.

For the bending mode with quanta v_b our theoretical energy differences are larger than those found experimentally, although the difference is no more than 10% for the three electronic states. Adding a second quanta in the bending mode shows that anharmonic contributions are non-negligible. We also corroborate the DFT and 2D-DVR results of Nguyen *et al.* [28]. Nguyen’s DFT results are based on the harmonic approximation.

The vibrational wavefunctions are used to compute FCFs among various pairs of ionic states. Their values and trends were presented in subsection “Wavefunction overlaps”. Additional bound-state energies and wavefunctions are shown in Supplementary Figures 1-3.

We can also quantify the quality of our potentials by a comparison of the dissociation energy and permanent dipole moments. The dissociation energy of the $(0,0,0)$ vibrational state of our $1^2A'(X^2\Sigma^+)$ potential is $D_0/hc = 33.3 \times 10^3 \text{ cm}^{-1}$ and compares favorably with the experimental measurements ranging from $32.3 \times 10^3 \text{ cm}^{-1}$ to $36.0 \times 10^3 \text{ cm}^{-1}$ [47–49]. Our determination of the permanent dipole moments of the $1^2A'(X^2\Sigma^+)$, $2^2A'(A^2\Pi)$, and $3^2A'(B^2\Sigma^+)$ states at their equilibrium geometries are 1.57 Debye, 0.314 Debye, and 0.396 Debye, respectively. Reference [50] measured 1.900(14) Debye and 0.396(61) Debye for the $(0,0,0)$ vibrational state of the $1^2A'(X^2\Sigma^+)$ and $3^2A'(B^2\Sigma^+)$ potentials. The agreement is mixed. A direct comparison for the $2^2A'(A^2\Pi)$ state can not be made as Ref. [50] presented a

fine-structure resolved measurement, i.e. they found permanent dipole moments of 0.590(45) Debye and 0.424(5) Debye for $\Omega = 1/2$ and $3/2$, respectively, suggesting that our value is too small. (The numbers in parenthesis are one-standard-deviation uncertainties in the last digits.)

Data Availability

The data sets generated during the current study are partially included in this published article (and its Supplementary Note 1) and also available from the corresponding author on reasonable request.

Acknowledgment

Work at Temple University is supported by the Army Research Office Grant No. W911NF-17-1-0563, the U.S. Air Force Office of Scientific Research Grant No. FA9550-14-1-0321 and the NSF Grant No. PHY-1908634.

Authors Contributions

S. K. conceived, designed, coordinated the work, and wrote the manuscript. Electronic structure calculations were performed by J. K., M. L. and A. P. Fitting of the potentials were performed by J. K and M. L. Bound states, wavefunctions and Franck-Condon factors calculations were performed by J. K. All authors contributed to the interpretation of the data and discussed the results.

Competing Interests

The authors declare no competing interests.

-
- [1] C. E. Wieman, D. E. Pritchard, and D. J. Wineland, “Atom cooling, trapping, and quantum manipulation,” in *More Things in Heaven and Earth: A Celebration of Physics at the Millennium*, edited by B. Bederson (Springer New York, New York, NY, 1999) pp. 426–441.
 - [2] P. I. Presunka and J. A. Coxon, “Laser excitation and dispersed fluorescence investigations of the $A^2\Pi-X^2\Sigma^+$ system of SrOH,” *Chem. Phys.* **190**, 97–111 (1995).
 - [3] R. F. Wormsbecher, R. E. Penn, and D. O. Harris, “High-resolution laser spectroscopy of

- CaNH₂: Analysis of the C²A₁-X²A₁ system,” J. Mol. Spec. **97**, 65–72 (1983).
- [4] R. F. Wormsbecher, M. Trkula, C. Martner, R. E. Penn, and D. O. Harris, “Chemiluminescent reactions of alkaline-earth metals with water and hydrazine,” J. Mol. Spec. **97**, 29–36 (1983).
- [5] R. C. Hilborn, Z. Qingshi, and D. O. Harris, “Laser spectroscopy of the A-X transitions of CaOH and CaOD,” J. Mol. Spec. **97**, 73–91 (1983).
- [6] P.F. Bernath and S. Kinsey-Nielsen, “Dye laser spectroscopy of the B²Σ⁺-X²Σ⁺ transition of CaOH,” Chem. Phys. Lett. **105**, 663–666 (1984).
- [7] C. R. Brazier and P. F. Bernath, “Observation of gas phase organometallic free radicals: Monomethyl derivatives of calcium and strontium,” J. Chem. Phys. **86**, 5918–5922 (1987).
- [8] A. M. R. P. Bopegedera, C. R. Brazier, and P. F. Bernath, “Laser spectroscopy of strontium and calcium monoalkylamides,” J. Phys. Chem. **91**, 2779–2781 (1987).
- [9] C. R. Brazier and P. F. Bernath, “The A²Π-x²Σ⁺ transition of monomethyl calcium: A rotational analysis,” J. Chem. Phys. **91**, 4548–4554 (1989).
- [10] P. F. Bernath, “Gas-phase inorganic chemistry: monovalent derivatives of calcium and strontium,” Science **254**, 665–670 (1991).
- [11] J. Nakagawa, R. F. Wormsbecher, and D. O. Harris, “High-resolution laser excitation spectra of linear triatomic molecules: Analysis of the B²Σ⁺-X²Σ⁺ system of SrOH and SrOD,” J. Mol. Spec. **97**, 37–64 (1983).
- [12] C. W. Bauschlicher Jr. and S. R. Langhoff, “*Ab initio* study of the alkali and alkaline-earth monohydroxides,” J. Chem. Phys. **84**, 901–909 (1998).
- [13] J. Dalibard and C. Cohen-Tannoudji, “Dressed-atom approach to atomic motion in laser light: the dipole force revisited,” J. Opt. Soc. Am B **2**, 1707–1720 (1985).
- [14] E. B. Norrgard, D. J. McCarron, M. H. Steinecker, M. R. Tarbutt, and D. DeMille, “Submillikelvin dipolar molecules in a radio-frequency magneto-optical trap,” Phys. Rev. Lett. **116**, 063004 (2016).
- [15] L. Anderegg, B. L. Augenbraun, E. Chae, B. Hemmerling, N. R. Hutzler, A. Ravi, A. Collopy, J. Ye, W. Ketterle, and J. M. Doyle, “Radio frequency magneto-optical trapping of CaF with high density,” Phys. Rev. Lett. **119**, 103201 (2017).
- [16] S. Truppe, H. J. Williams, M. Hambach, L. Caldwell, N. J. Fitch, E. A. Hinds, B. E. Sauer, and M. R. Tarbutt, “Molecules cooled below the Doppler limit,” Nature Physics **13**, 1173 (2017).

- [17] Alejandra L. Collopy, Shiqian Ding, Yewei Wu, Ian A. Finneran, Loïc Anderegg, Benjamin L. Augenbraun, John M. Doyle, and Jun Ye, “3d magneto-optical trap of yttrium monoxide,” *Phys. Rev. Lett.* **121**, 213201 (2018).
- [18] J. Lim, J. R. Almond, M. A. Trigatzis, J. A. Devlin, N. J. Fitch, B. E. Sauer, M. R. Tarbutt, and E. A. Hinds, “Laser cooled ybf molecules for measuring the electron’s electric dipole moment,” *Phys. Rev. Lett.* **120**, 123201 (2018).
- [19] Timur A. Isaev and Robert Berger, “Polyatomic candidates for cooling of molecules with lasers from simple theoretical concepts,” *Phys. Rev. Lett.* **116**, 063006 (2016).
- [20] I. Kozyryev, L. Baum, K. Matsuda, B. L. Augenbraun, L. Anderegg, A. P. Sedlack, and J. M. Doyle, “Sisyphus laser cooling of a polyatomic molecule,” *Phys. Rev. Lett.* **118**, 173201 (2017).
- [21] Ivan Kozyryev, Timothy C. Steimle, Phelan Yu, Duc-Trung Nguyen, and John M. Doyle, “Determination of CaOH and CaOCH₃ vibrational branching ratios for direct laser cooling and trapping,” *New J. Phys.* **21**, 052002 (2019).
- [22] Jacek Klos and Svetlana Kotochigova, “Prospects for laser cooling of polyatomic molecules with increasing complexity,” (2019), in preparation.
- [23] I. Kozyryev, L. Baum, K. Matsuda, and J. M. Doyle, “Proposal for laser cooling of complex polyatomic molecules,” *Chem. Phys. Chem.* **17**, 3641–3648 (2016).
- [24] D. R. Yarkony, “Diabolical conical intersections,” *Rev. Mod. Phys.* **68**, 985–1013 (1996).
- [25] M. Kas, J. Loreau, J. Lievin, and N. Vaeck, “*Ab initio* study of the neutral and anionic alkali and alkaline earth hydroxides: Electronic structure and prospects for sympathetic cooling of OH⁻,” *J. Chem. Phys.* **146**, 194309 (2017).
- [26] Giannoula Theodorakopoulos, Ioannis Petsalakis, and Ian Hamilton, “*Ab initio* calculations on the ground and excited states of BeOH and MgOH,” *J. Chem. Phys.* **111**, 10484–10490 (1999).
- [27] Paul I. Presunka and John A. Coxon, “Laser spectroscopy of the $\tilde{A}^2\Pi - \tilde{X}^2\Sigma^+$ transition of SrOH: Deperturbation analysis of Kresonance in the $v_2=1$ level of the $\tilde{A}^2\Pi$,” *J. Chem. Phys.* **101**, 201–222 (1994).
- [28] Duc-Trung Nguyen, Timothy C. Steimle, Ivan Kozyryev, Meng Huang, and Anne B. McCoy, “Fluorescence branching ratios and magnetic tuning of the visible spectrum of SrOH,” *J. Mol. Spec.* **347**, 7 – 18 (2018).

- [29] M. V. Berry, “Quantum phase factors accompanying adiabatic changes,” *Proc. R. Soc. Lond. A* **392**, 45–57 (1984).
- [30] Changjian Xie, Brian K. Kendrick, David R. Yarkony, and Huo Guo, “Constructive and destructive interference in nonadiabatic tunneling via conical intersection,” *J. Chem. Theory Comput* **13**, 1902–1910 (2017).
- [31] M. Born and R. Oppenheimer, “Zur quantentheorie der molekeln,” *Ann. Phys.* **84**, 457 (1927).
- [32] W. Domcke, D. Yarkony, and H. Köppel, *Conical Intersections: Electronic Structure, Dynamics & Spectroscopy*, Advanced series in physical chemistry (World Scientific, Singapore, 2004).
- [33] Evgueni E. Nikitin, “Adiabatic and diabatic collision processes at low energies,” in *Springer Handbooks of Atomic, Molecular, and Optical Physics*, edited by Gordon W. F. Drake (Springer, New York, 2006) Chap. 49, pp. 741–752.
- [34] Hiroshi Akima, “A new method of interpolation and smooth curve fitting based on local procedures,” *J. ACM* **17**, 589–602 (1970).
- [35] R. Renner, “Zur theorie der wechselwirkung zwischen elektronen- und kernbewegung bei dreiatomigen, stabförmigen molekülen,” *Zeitschrift für Physik* **92**, 172–193 (1934).
- [36] G. Herzberg and E. Teller, “Schwingungsstruktur der elektronenübergänge bei mehratomigen molekülen,” *Zeitschrift für Physikalische Chemie* **21B**, 410–446 (1933).
- [37] J. F. Stanton, J. Gauss, L. Cheng, M. E. Harding, D. A. Matthews, and P. G. Szalay, “CFOUR, Coupled-Cluster techniques for Computational Chemistry, a quantum-chemical program package,” With contributions from A.A. Auer, R.J. Bartlett, U. Benedikt, C. Berger, D.E. Bernholdt, Y.J. Bomble, O. Christiansen, F. Engel, R. Faber, M. Heckert, O. Heun, M. Hilgenberg, C. Huber, T.-C. Jagau, D. Jonsson, J. Jusélius, T. Kirsch, K. Klein, W.J. Lauderdale, F. Lipparini, T. Metzroth, L.A. Mück, D.P. O’Neill, D.R. Price, E. Prochnow, C. Puzzarini, K. Ruud, F. Schiffmann, W. Schwalbach, C. Simmons, S. Stopkowitz, A. Tajti, J. Vázquez, F. Wang, J.D. Watts and the integral packages MOLECULE (J. Almlöf and P.R. Taylor), PROPS (P.R. Taylor), ABACUS (T. Helgaker, H.J. Aa. Jensen, P. Jørgensen, and J. Olsen), and ECP routines by A. V. Mitin and C. van Wüllen. For the current version, see <http://www.cfour.de>.
- [38] F. Weigend and R. Ahlrichs, “Balanced basis sets of split valence, triple zeta valence and quadruple zeta valence quality for H to Rn: Design and assessment of accuracy,” *Phys. Chem.*

- Chem. Phys. **7**, 3297–3305 (2005).
- [39] Ivan S. Lim, Hermann Stoll, and Peter Schwerdtfeger, “Relativistic small-core energy-consistent pseudopotentials for the alkaline-earth elements from Ca to Ra,” *J. Chem. Phys.* **124**, 034107 (2006).
- [40] Thom H. Dunning, “Gaussian basis sets for use in correlated molecular calculations. i. The atoms boron through neon and hydrogen,” *J. Chem. Phys.* **90**, 1007–1023 (1989).
- [41] Yihan Shao, Zhengting Gan, Evgeny Epifanovsky, Andrew T.B. Gilbert, Michael Wormit, Joerg Kussmann, Adrian W. Lange, Andrew Behn, Jia Deng, Xintian Feng, Debashree Ghosh, Matthew Goldey, Paul R. Horn, Leif D. Jacobson, Ilya Kaliman, Rustam Z. Khaliiullin, Tomasz Kuś, Arie Landau, Jie Liu, Emil I. Proynov, Young Min Rhee, Ryan M. Richard, Mary A. Rohrdanz, Ryan P. Steele, Eric J. Sundstrom, H. Lee Woodcock III, Paul M. Zimmerman, Dmitry Zuev, Ben Albrecht, Ethan Alguire, Brian Austin, Gregory J. O. Beran, Yves A. Bernard, Eric Berquist, Kai Brandhorst, Ksenia B. Bravaya, Shawn T. Brown, David Casanova, Chun-Min Chang, Yunqing Chen, Siu Hung Chien, Kristina D. Closser, Deborah L. Crittenden, Michael Diedenhofen, Robert A. DiStasio Jr., Hainam Do, Anthony D. Dutoi, Richard G. Edgar, Shervin Fatehi, Laszlo Fusti-Molnar, An Ghysels, Anna Golubeva-Zadorozhnaya, Joseph Gomes, Magnus W.D. Hanson-Heine, Philipp H.P. Harbach, Andreas W. Hauser, Edward G. Hohenstein, Zachary C. Holden, Thomas-C. Jagau, Hyunjun Ji, Benjamin Kaduk, Kirill Khistyayev, Jaehoon Kim, Jihan Kim, Rollin A. King, Phil Klunzinger, Dmytro Kosenkov, Tim Kowalczyk, Caroline M. Krauter, Ka Un Lao, Adèle D. Laurent, Keith V. Lawler, Sergey V. Levchenko, Ching Yeh Lin, Fenglai Liu, Ester Livshits, Rohini C. Lochan, Arne Luenser, Prashant Manohar, Samuel F. Manzer, Shan-Ping Mao, Narbe Mardirossian, Aleksandr V. Marenich, Simon A. Maurer, Nicholas J. Mayhall, Eric Neuscamman, C. Melania Oana, Roberto Olivares-Amaya, Darragh P. O’Neill, John A. Parkhill, Trilisa M. Perrine, Roberto Peverati, Alexander Prociuk, Dirk R. Rehn, Edina Rosta, Nicholas J. Russ, Shaama M. Sharada, Sandeep Sharma, David W. Small, Alexander Sodt, Tamar Stein, David Stück, Yu-Chuan Su, Alex J.W. Thom, Takashi Tsuchimochi, Vitalii Vanovschi, Leslie Vogt, Oleg Vydrov, Tao Wang, Mark A. Watson, Jan Wenzel, Alec White, Christopher F. Williams, Jun Yang, Sina Yeganeh, Shane R. Yost, Zhi-Qiang You, Igor Ying Zhang, Xing Zhang, Yan Zhao, Bernard R. Brooks, Garnet K.L. Chan, Daniel M. Chipman, Christopher J. Cramer, William A. Goddard III, Mark S. Gordon, Warren J. Hehre, Andreas Klamt, Henry

- F. Schaefer III, Michael W. Schmidt, C. David Sherrill, Donald G. Truhlar, Arieh Warshel, Xin Xu, Alán Aspuru-Guzik, Roi Baer, Alexis T. Bell, Nicholas A. Besley, Jeng-Da Chai, Andreas Dreuw, Barry D. Dunietz, Thomas R. Furlani, Steven R. Gwaltney, Chao-Ping Hsu, Yousung Jung, Jing Kong, Daniel S. Lambrecht, WanZhen Liang, Christian Ochsenfeld, Vitaly A. Rassolov, Lyudmila V. Slipchenko, Joseph E. Subotnik, Troy Van Voorhis, John M. Herbert, Anna I. Krylov, Peter M.W. Gill, and Martin Head-Gordon, "Advances in molecular quantum chemistry contained in the Q-Chem 4 program package," *Mol. Phys.* **113**, 184–215 (2015).
- [42] Huidong Li, Hao Feng, Weiguo Sun, Yi Zhang, Qunchao Fan, Kirk A. Peterson, Yaoming Xie, and Henry F. Schaefer III, "The alkaline earth dimer cations (Be_2^+ , Mg_2^+ , Ca_2^+ , Sr_2^+ , and Ba_2^+). Coupled cluster and full configuration interaction studies," *Mol. Phys.* **111**, 2292–2298 (2013).
- [43] H.-J. Werner, P. J. Knowles, G. Knizia, F. R. Manby, and M. Schütz, "Molpro: a general purpose quantum chemistry program package," *Comput. Mol. Sci.* **2**, 242–253 (2012).
- [44] T.-S. Ho and H. Rabitz, "A general method for constructing multidimensional molecular potential energy surfaces from *ab initio* calculations," *J. Chem. Phys.* **104**, 2584 (1996).
- [45] P.I. Presunka and J.A. Coxon, "High-resolution laser spectroscopy of excited bending vibrations ($u_2 \leq 2$) of the $\tilde{\text{B}}^2\Sigma^+$ and $\tilde{\text{X}}^2\Sigma^+$ electronic states of SrOH: Analysis of *l*-type doubling and *l*-type resonance," *Can. J. Chem.* **71**, 1689–1705 (1993).
- [46] M. D. Oberlander and J. M. Parson, "Laser excited fluorescence study of reactions of excited Ca and Sr with water and alcohols: Product selectivity and energy disposal," *J. Chem. Phys.* **105**, 5806–5816 (1996).
- [47] J. van der Hurk, Tj. Hollander, and C.Th.J. Alkemade, "Excitation energies of strontium mono-hydroxide bands measured in flames," *J. Quant. Spectrosc. and Radiat. Transf.* **14**, 1167 – 1178 (1974).
- [48] D. H. Cotton and D. R. Jenkins, "Dissociation energies of gaseous alkaline earth hydroxides," *Trans. Faraday Soc.* **64**, 2988–2997 (1968).
- [49] Edmond Murad, "Thermochemical properties of the gaseous alkaline earth monohydroxides," *J. Chem. Phys.* **75**, 4080–4085 (1981).
- [50] T. C. Steimle, D. A. Fletcher, K. Y. Jung, and C. T. Scurlock, "A supersonic molecular beam optical stark study of caoh and sroh," *J. Chem. Phys.* **96**, 2556–2564 (1992).

Supplementary Material

Supplementary Note 1: Stretching and bending modes in the ground and excited state potentials. We have used a distributed Gaussian basis approach to obtain the energies and wavefunctions of the lowest few $J = 0$ and 1 stretching and bending modes in each of the $1^2A'(X^2\Sigma^+)$, $1^2A''(A^2\Pi)$, and $3^2A'(B^2\Sigma^+)$ PESs. Supplementary Figures 8, 9, and 10 show contour plots of the real-valued vibrational wavefunctions for bending and stretching state progressions for these three PESs. One can identify bending and stretching quantum numbers, v_b and v_s , by counting the lobes or studying the nodal pattern of the wavefunctions in θ and R directions, indicating that for the lowest energies the bending and stretching modes are not mixed. Positive and negative parity states have an even and odd symmetry with respect to the reflection $\theta \rightarrow 180^\circ - \theta$ and, thus, whether v_b is even or odd. Laser cooling is performed from the $J = 1, p = +1 (0, 0, 0)$ state of the $1^2A'(X^2\Sigma^+)$ potential. We show this state in the left upper corner of Supplementary Figure 8. It lies approximately 0.5 cm^{-1} above the absolute rovibrational ground state with $J = 0$, corresponding to a $2B_0$ of excitation energy, where B_0 is a rotational constant of SrOH $1^2A'(X^2\Sigma^+)$.

Franck-Condon factors of vibronic transitions, the square of the overlap of vibrational wavefunctions, among the lowest bending and stretching modes of $1^2A'(X^2\Sigma^+)$, $1^2A''(A^2\Pi)$, and $3^2A'(B^2\Sigma^+)$ are shown in Supplementary Tables IV, V, and VI.

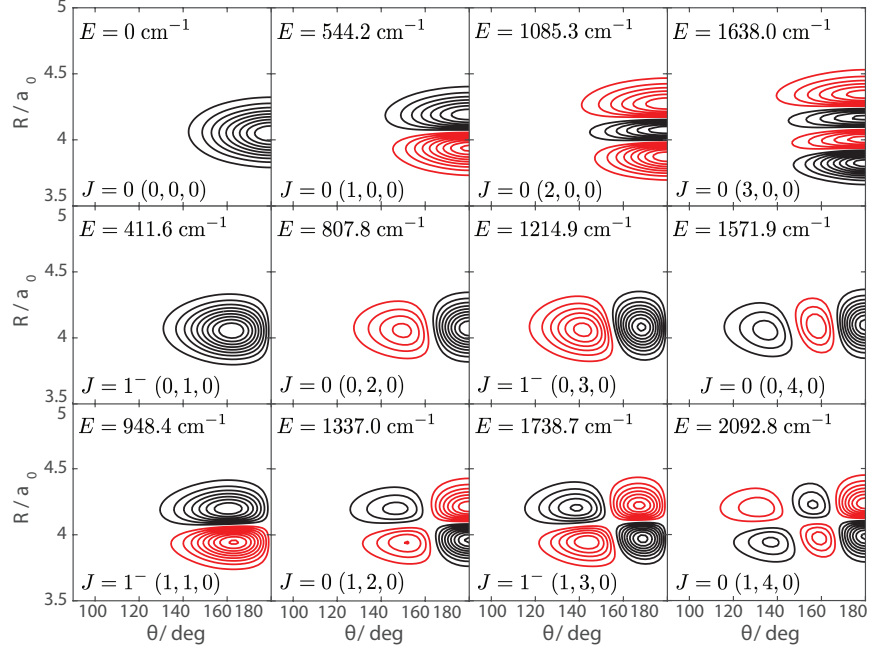


FIG. 8. Contour plots of wavefunctions of J^p ro-vibrational bound states as functions of separation R and angle θ for total angular momentum $J = 1$ and parity $p = \pm 1$ of the $1^2A'(X^2\Sigma^+)$ ground-state potential energy surface. Triplets $(v_s, v_b, v_{\text{OH}} = 0)$ indicate stretching and bending quantum numbers. Black and red lines denote wavefunction contours of opposite sign, respectively. Positive and negative parity states have an even and odd symmetry with respect to the reflection of angle $\theta \rightarrow 180^\circ - \theta$. Energies in units of cm^{-1} are given with respect to the $J^p = 0^+ (0, 0, 0)$ level.

TABLE II. Franck-Condon factors between pairs of $(v_s, v_b, 0)$ rovibrational SrOH states of $J = 0$ $2^2A'(A^2\Pi)$, $J = 0$ $3^2A'(B^2\Sigma^+)$, and $J = 1$ $1^2A'(X^2\Sigma^+)$. In the table the three states are denoted by A, B and X, respectively. Here parity $p = +1$ or -1 corresponds to whether v_b is even or odd.

A\X	(000)	(100)	(200)	(300)	(010)	(110)
(000)	0.940	0.058				
(100)	0.056	0.829	0.112	0.003		
(200)	0.003	0.104	0.736	0.151		
(300)		0.007	0.136	0.640		
(010)					0.941	0.057
(110)					0.055	0.832
B\X	(000)	(100)	(200)	(300)	(010)	(110)
(000)	0.993	0.006				
(100)	0.006	0.981	0.011			
(200)		0.011	0.969	0.017		
(300)			0.017	0.962		
(010)					0.994	0.004
(110)					0.004	0.984
A\B	(000)	(100)	(200)	(300)	(010)	(110)
(000)	0.969	0.030				
(100)	0.028	0.911	0.060			
(200)	0.002	0.053	0.862	0.081		
(300)		0.004	0.067	0.795		
(010)					0.967	0.033
(110)					0.031	0.902

TABLE III. Comparison of energies for three $(v_s, v_b, 0)$ stretching and bending levels with total angular momentum $J = 0$ and parity $+1$ for the $1^2A'(X^2\Sigma^+)$, $1^2A''(A^2\Pi)$, and $3^2A'(B^2\Sigma^+)$ states of the $^{88}\text{Sr}-^{16}\text{O}^1\text{H}$ isotopologue using our diabatic and adiabatic potential energy surfaces, and data from the literature. Energies are relative to that of the $(0, 0, 0)$ mode and in units of cm^{-1} .

Method	(1, 0, 0)	(0, 1, 0)	(0, 2, 0)
$1^2A'(X^2\Sigma^+)$			
CCSD(T)	524	382	748
2D-DVR [28]	-	322	638
Exp. [45]	527	364	703
$1^2A''(A^2\Pi)$			
CCSD(T)	544	412	808
2D-DVR [28]	-	308	614
Exp. [45]	543	-	-
Exp. [2]	-	378	-
$3^2A'(B^2\Sigma^+)$			
EOM-	549	417	799
CCSD(dT)			
2D-DVR [28]	-	358	699
Exp. [46]	536	-	-
Exp. [45]	-	401	771

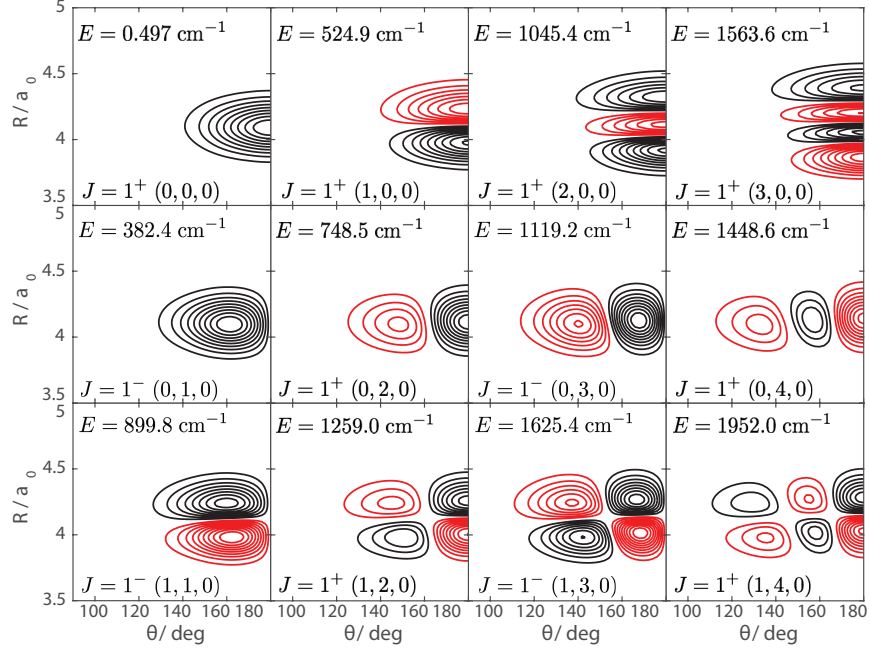


FIG. 9. Contour plots of wavefunctions of rovibrational bound states as functions of separation R and angle θ for $J^p = 0^+$ and 1^\pm levels of the $1^2A''(A^2\Pi)$ potential energy surface. Energies in units of cm^{-1} are given with respect to the $J^p = 0^+ (0,0,0)$ level.

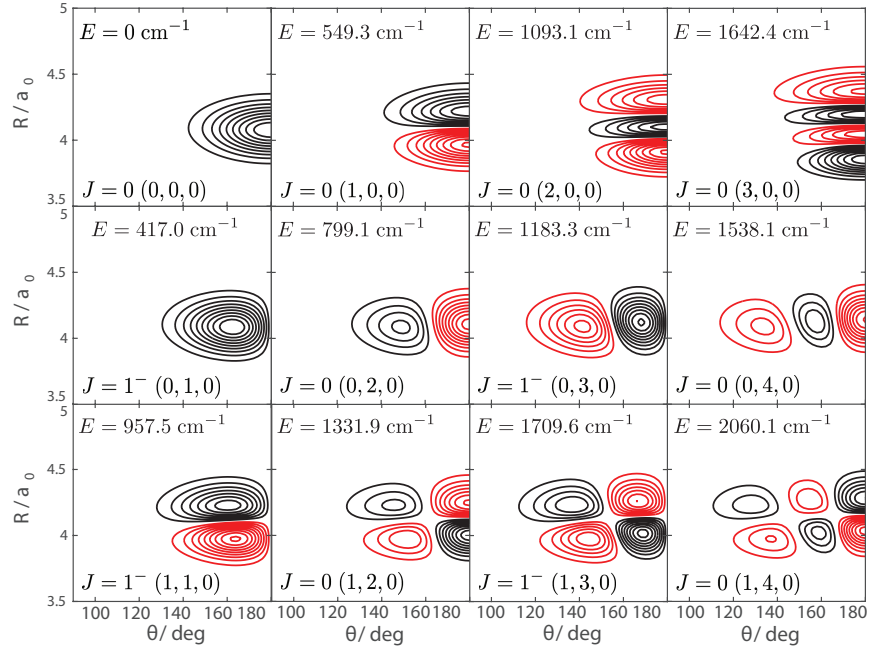


FIG. 10. Contour plots of wavefunctions of rovibrational bound states as functions of separation R and angle θ for $J^p = 0^+$ and 1^\pm levels of the $3^2A'(B^2\Sigma^+)$ potential energy surface. Energies in units of cm^{-1} are given with respect to the $J^p = 0^+ (0,0,0)$ level.

TABLE IV. Matrix of Franck-Condon factors (FCFs) between $(v_s, v_b, 0)$ and $(v'_s, v'_b, 0)$ SrOH rovibrational states of the excited $J = 0$ $1^2A''(A^2\Pi)$ and ground $J = 1$ $1^2A'(X^2\Sigma^+)$ states, respectively. Only FCFs larger than 10^{-3} are shown.

A\X	(000)	(100)	(200)	(300)	(010)	(020)	(030)	(040)	(110)	(120)	(130)	(140)
(000)	0.940	0.058										
(100)	0.056	0.829	0.112	0.003								
(200)	0.003	0.104	0.736	0.151								
(300)		0.007	0.136	0.640								
(010)					0.941				0.057			
(020)						0.940				0.057		
(030)							0.942				0.054	
(040)								0.942				0.051
(110)					0.055				0.832			
(120)						0.055				0.832		
(130)							0.052				0.839	
(140)								0.049				0.844

TABLE VI. Matrix of Franck-Condon factors (FCFs) between $(v_s, v_b, 0)$ and $(v'_s, v'_b, 0)$ SrOH rovibrational levels of the excited $J = 0$ $1^2A''(A^2\Pi)$ and $J = 0$ $3^2A'(B^2\Sigma^+)$ states, respectively. Only FCFs larger than 10^{-3} are shown.

A\B	(000)	(100)	(200)	(300)	(010)	(020)	(030)	(040)	(110)	(120)	(130)	(140)
(000)	0.969	0.030										
(100)	0.028	0.911	0.060									
(200)	0.002	0.053	0.862	0.081								
(300)		0.004	0.067	0.795								
(010)					0.967				0.033			
(020)						0.963				0.036		
(030)							0.963				0.035	
(040)								0.955		0.002		0.041
(110)					0.031		0.002		0.902			
(120)						0.034		0.002		0.891		
(130)							0.032				0.887	
(140)								0.040				0.862